Radiative Impacts of the 2011 Abrupt Drops in Water Vapor and Ozone in the Tropical Tropopause Layer

Radiative Impacts of the 2011 Abrupt Drops in Water Vapor and Ozone in the Tropical Tropopause Layer

DANIEL M. GILFORD AND SUSAN SOLOMON

Department of Earth, Atmospheric and Planetary Sciences, Massachusetts Institute of Technology, Cambridge, Massachusetts

ROBERT W. PORTMANN

National Oceanic and Atmospheric Administration/Earth System Research Laboratory/Chemical Sciences Division, Boulder, Colorado

(Manuscript received 2 March 2015, in final form 21 October 2015)

ABSTRACT

An abrupt drop in tropical tropopause layer (TTL) water vapor, similar to that observed in 2000, recently occurred in 2011, and was concurrent with reductions in TTL temperature and ozone. Previous studies have indicated that such large water vapor variability can have significant radiative impacts. This study uses *Aura* Microwave Limb Sounder observations, the Stratospheric Water Vapor and Ozone Satellite Homogenized dataset, and two radiative transfer models to examine the radiative effects of the observed changes in TTL water vapor and ozone on TTL temperatures and global radiative forcing (RF). The analyses herein suggest that quasi-isentropic poleward propagation of TTL water vapor reductions results in a zonal-mean structure with ''wings'' of extratropical water vapor reductions, which account for about half of the 2011 abrupt drop global radiative impact. RF values associated with the mean water vapor concentrations differences between 2012/13 and 2010/11 are between -0.01 and -0.09 W m^{-2}, depending upon the altitude above which perturbations are considered. TTL water vapor and ozone variability during this period jointly lead to a transient radiative cooling of ~0.25–0.5 K in layers below the tropopause. The 2011 abrupt drop also prolonged the reduction in stratospheric water vapor that followed the 2000 abrupt drop, providing a longer-term radiative forcing of climate. Water vapor concentrations from 2005 to 2013 are lower than those from 1990 to 1999, resulting in a RF between these periods of about -0.045 W m^{-2}, approximately 12% as large as, but of opposite sign to, the concurrent estimated CO_2 forcing.

1. Introduction

Transport of air from the troposphere to the stratosphere largely occurs across the tropical tropopause layer (TTL), typically located between 20°S and 20°N and from 150 to 70 hPa (Fueglistaler et al. 2009). Water vapor and ozone concentrations vary in the TTL as air parcels cross the cold-point tropopause (CPT; ~90 hPa) into the stratosphere, and have been shown to have substantial radiative impacts within the lower stratosphere and on the troposphere below (e.g., Forster and Shine 1999; Gettelman et al. 2004; Randel et al. 2006; Solomon et al. 2010; Maycock et al. 2014). In this paper, we examine the local and nonlocal radiative effects associated with a recently observed 2011 sudden drop in TTL water vapor (Dessler et al. 2013; Urban et al. 2014; Dessler et al. 2014) that was accompanied by reductions in temperature and ozone. We also examine the radiative effects of longer-term changes in water vapor from 1990 through 2013.

A sudden reduction in TTL water vapor was observed in 2000, and was described by Randel et al. (2006) as an ''abrupt drop.'' They showed that the water vapor reductions were also associated with reductions in ozone, reductions in temperature, and increases in TTL upwelling circulation. Their model results showed that idealized ozone reductions in a single lower stratospheric layer played a radiative role in the local 2000 temperature reductions, but nonlocal radiative impacts on layers below the reductions were not fully assessed.

Corresponding author address: Daniel M. Gilford, Department of Earth, Atmospheric and Planetary Sciences, Massachusetts Institute of Technology, 77 Massachusetts Avenue, Cambridge, MA 02139.
Email: dgilford@mit.edu

DOI: 10.1175/JCLI-D-15-0167.1

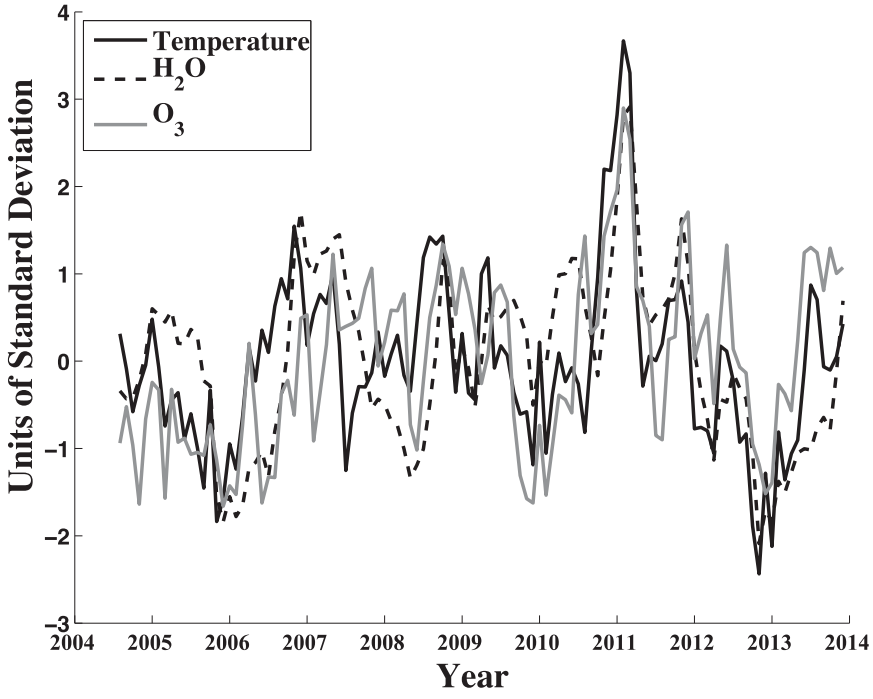

FIG. 1. Standardized monthly time series of temperature (solid black curve), water vapor (dashed black curve), and ozone (gray curve) deseasonalized anomalies from 2005–13 *Aura* MLS observations averaged over 20°S–20°N at 82 hPa.

Solomon et al. (2010) explored the radiative effects of water vapor reductions during the 2000 abrupt drop and found decreases in net downwelling LW radiation at the tropopause (a negative climate radiative forcing of $-0.098\,\mathrm{W\,m^{-2}}$), suggesting a contribution to the "slowdown" of global warming during 2000–09. Other studies (e.g., Forster and Shine 1999; Shindell 2001; Forster and Shine 2002; Joshi and Jones 2009; Tian et al. 2009; Joshi et al. 2010; Maycock et al. 2011; Dessler et al. 2013; Maycock et al. 2014) have similarly shown that lower stratospheric water vapor is radiatively important for surface as well as stratospheric climate.

In addition to the notable 2000 reductions, another such abrupt drop in water vapor occurred in 2011/12 (Dessler et al. 2013; Urban et al. 2014; Dessler et al. 2014), again accompanied by reductions in TTL temperatures and ozone concentrations. Following the 2000 abrupt drop, water vapor concentrations remained relatively low compared with 1990–99 concentrations (see section 3d) but increased to a peak in September 2011 before suddenly dropping to a local minimum anomaly in May 2013 (Fig. 1); herein for convenience we refer to this ~21-month variability event (maximum to minimum) as the "2011 abrupt drop." The 2011 abrupt drop provides a unique opportunity to explore the structure of such changes and to assess its radiative impacts on climate and tropospheric temperatures, due to improved data coverage compared to the earlier event in 2000. The advent of the *Aura* Microwave Limb Sounder (MLS; NASA 2006) offers a robust dataset with which to characterize this recent 2011 abrupt drop event. *Aura* MLS measurements are an improvement on the earlier Halogen Occultation Experiment (HALOE) record because they have increased horizontal resolution and accurate observations of ozone and water vapor in the TTL (Livesey et al. 2011; Hegglin et al. 2013; Tegtmeier et al. 2013).

The TTL radiative time scale ranges from 15 to 100 days (e.g., Fueglistaler et al. 2009), a time scale shorter than the ~21-month period of the 2011 abrupt drop. This suggests that short-term radiative adjustments associated with the 2011 abrupt drop would have impacted atmospheric temperatures. Furthermore, the long-term radiative impacts on the climate system could be important if relatively low concentrations persist. Here we show that water vapor concentrations in the period of MLS observations from 2005 to 2013 have remained low relative to the 1990–99 period (see Fig. 9), leading to a long-term negative radiative forcing on the troposphere that is in part related to the 2011 abrupt drop. The structure of the 2011 abrupt drop is characterized in this paper, and the radiative effects of TTL concentration changes (both short term and long term) are investigated using raw *Aura* MLS observations and

the combined Stratospheric Water Vapor and Ozone Satellite Homogenized (SWOOSH) dataset (Davis and Rosenlof 2013), along with two radiative transfer models.

The largest perturbations in water vapor and ozone during the 2011 abrupt drop are found at or just below the CPT altitude. The ''substratosphere'' (Folkins et al. 1999, 2000; Thuburn and Craig 2002)—a region of the TTL defined as above the main convective outflow level (typically ~150 hPa) and below the CPT (~90 hPa)—is a region where temperature variability is radiatively rather than dynamically dominated, and generally small in magnitude compared with the variability at and above the CPT (Randel and Wu 2015). Thus, short-term radiative adjustments related to TTL chemical constituent perturbations could be an important contribution to temperature variability in the substratosphere. A goal of this study is to ascertain the magnitude of substratospheric radiative temperature adjustments associated with the 2011 abrupt drops in water vapor and ozone.

This paper is organized as follows. Section 2 describes the data used in this study, defines the 2011 abrupt drop, and analyzes the abrupt drop structure. The three-dimensional structure of the abrupt drop is used to perturb TTL ozone and water vapor concentrations in two offline radiative transfer models. In section 3, we describe the radiative transfer models and study methods, and present the radiative forcing and resulting temperature adjustments associated with the abrupt drop perturbations. Furthermore, the role of the 2011 abrupt drop is examined in the context of the long-term changes in water vapor and the associated radiative forcing over about the past two decades. A summary of study results follows in section 4.

2. Abrupt drop analysis

a. Satellite observations and TTL relationships

This study uses measurements of water vapor, ozone, and temperature from the *Aura* Microwave Limb Sounder level-2 version 3.3 dataset (Livesey et al. 2011) from 2005 to 2013. Satellite swaths are quality controlled according to NASA's quality field recommendations and are regridded onto a 5° × 5° horizontal grid. For water vapor there are 31 recommended useful vertical levels from 316 to 1 hPa, whereas for ozone and temperature there are 29 recommended useful vertical levels from 216 to 1 hPa. *Aura* MLS measurements of TTL water vapor and ozone generally compare well with multi-instrument means in comprehensive Stratosphere–Troposphere Processes and their Role in Climate (SPARC) instrument studies (Hegglin et al. 2013; Tegtmeier et al. 2013).

For analyses of satellite data earlier than the *Aura* MLS period (prior to 2005) and for analyses on isentropic surfaces, we use observations from the SWOOSH dataset (Davis and Rosenlof 2013). SWOOSH is a monthly and zonal-mean data product available on isentropic and pressure surfaces (identical to those of *Aura* MLS level-2 data), separated by every 2.5° latitude. The ''combined'' SWOOSH dataset homogenizes measurements from the HALOE, *UARS* MLS, SAGE-II, SAGE-III, and *Aura* MLS instruments to form a coherent observational dataset of stratospheric water vapor concentrations. To retain coherence between coincident space and time instrument measurements during the overlap time period (2004/05), the SWOOSH methodology adds corrective offsets to the HALOE, SAGE, and *UARS* MLS data to force agreement with *Aura* MLS [as in Solomon et al. (2010) and Maycock et al. (2014)]. These offsets vary in latitude and height but are constant in time. Following the discontinuation of HALOE and SAGE contributions in mid-2005, the SWOOSH combined dataset and *Aura* MLS measurements are identical.

The gridded *Aura* MLS data are used to examine the linkages between ozone, water vapor, and temperature in the TTL. At each grid point, monthly averages of temperature, water vapor, and ozone are deseasonalized to determine monthly anomalies. Time series of water vapor, ozone, and temperature anomalies at 82 hPa averaged zonally and meridionally over 20°S–20°N show significant correlations with one another in Fig. 1 (time series are standardized for illustration). Pearson correlation coefficients (R) between these time series are determined by first detrending the data. A null hypothesis that each correlation is significantly different from zero is tested with a two-sided Student's t test using an effective number of degrees of freedom accounting for the lag-1 autocorrelations of each individual time series (e.g., Bretherton et al. 1999; Santer et al. 2000; Bandoro et al. 2014). Correlation coefficients corresponding to these tropical time series (20°S–20°N, 2005–13) at each vertical level are shown in Fig. 2.

Ozone and temperatures in the TTL are linked both dynamically and radiatively. Anomalous increases in upwelling are associated with adiabatic decreases in temperature and act on the positive vertical gradient of ozone in the TTL, advecting ozone-poor air up from below and decreasing ozone mixing ratios (e.g., Randel et al. 2006; Schoeberl et al. 2008; Lamarque and Solomon 2010). Conversely, anomalous decreases in upwelling are associated with increases in temperature and increased ozone mixing ratios. The ozone perturbations have a positive radiative feedback, with negative ozone anomalies locally cooling the TTL and positive

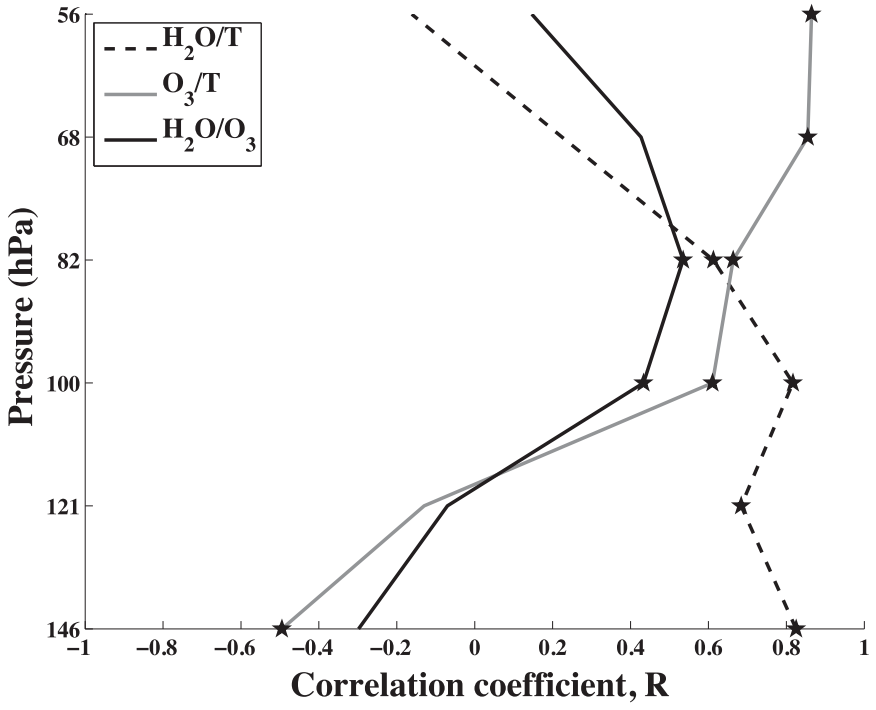

FIG. 2. TTL vertical profiles of correlation coefficients (R) between water vapor/temperature (dashed black curve), ozone/temperature (gray curve), and water vapor/ozone (solid black curve), calculated from detrended MLS observed monthly deseasonalized anomaly time series from 2005 to 2013 averaged over 20°S–20°N. Stars indicate correlations that are significant at 95% confidence, determined with a two-sided Student's t test and with the effective degrees of freedom adjusted to account for autocorrelation (see text).

ozone anomalies locally warming the TTL. This radiative feedback enhances the seasonal cycle of temperatures in the TTL, for instance, and long-term changes in TTL ozone can be associated with local long-term temperature trends (e.g., Folkins et al. 2006; Chae and Sherwood 2007; Fueglistaler et al. 2011; Polvani and Solomon 2012). Thus a notable portion of TTL temperature variability is due to ozone radiative effects, as a response to an initial change in TTL circulation. In accordance with these processes, Fig. 2 shows that ozone and temperature are significantly and positively correlated at levels near and above the CPT (100, 82, and 68 hPa). This relationship increases with height in the TTL, because of both the increasing ozone gradient with height and the increasing radiative influence of ozone on temperature at these altitudes. Relationships between dynamic influences and ozone concentrations during the 2011 abrupt drop are discussed further in section 2b.

Water vapor and temperature are significantly and positively correlated locally at and below the CPT (121, 100, and 82 hPa). Anomalously cold temperatures (related to adiabatic cooling through anomalous increased upwelling) reduce the water vapor content of parcels traveling up through the TTL and into the lower stratosphere (e.g., Dhomse et al. 2008); conversely, anomalous warm temperatures related to adiabatic warming through reduced upwelling lead to positive water vapor anomalies in the upward propagating parcels. Stratospheric water vapor can also vary in response to the ozone radiative feedback on temperatures discussed above, an additional mechanism of water vapor variability that has been shown to be radiatively important for tropospheric forcing (Stuber et al. 2001). Above 82 hPa in the tropics, the CPT has been traversed by upward propagating parcels and water vapor concentrations are near constant (with slight increases due to methane oxidation and mixing in of older stratospheric air; e.g., Fueglistaler et al. 2009). These parcels propagate further into the stratosphere in accordance with the concept of a tropical ''tape recorder'' (Mote et al. 1996), and poleward along quasi-isentropic surfaces (Holton et al. 1995, their section 2.2 and Fig. 4).

The correlations between water vapor and ozone deseasonalized anomalies at TTL heights show which regions of the TTL display linked changes in water vapor and ozone. We find that ozone and water vapor are significantly positively correlated over 100–82 hPa over the full period of record. If only 2011 and 2012 are

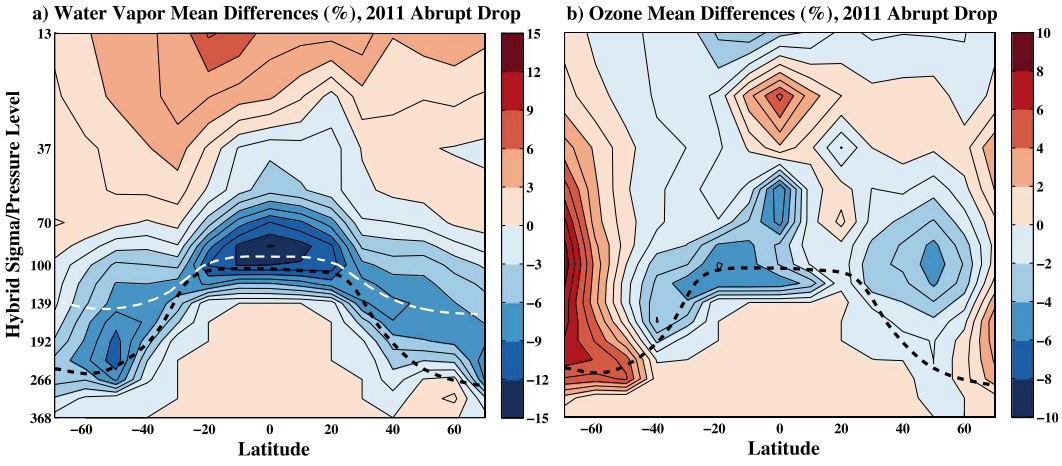

FIG. 3. Zonal-mean distribution of *Aura* MLS observed percent mean differences in (a) water vapor and (b) ozone during the 2011 abrupt drop (between 2012/13 and 2010/11 concentrations). These changes are used to perturb the radiative transfer model (PORT) and thus are shown on the PORT grid for comparison with radiation results, and down to one level below the tropopause for illustration. The dashed black curve is the zonal and annual mean tropopause. The dashed white curve is the 380-K zonal-mean isentropic surface averaged from 2010 to 2013. Contour intervals are 1.5% in (a) and 1% in (b).

considered, the vertical range of significant positive correlations increases to 121–68 hPa, suggesting a common origin in anomalous TTL upwelling during the 2011 abrupt drop.

b. 2011 Abrupt drop temporal and spatial structure

Following Rosenlof and Reid (2008) and Solomon et al. (2010) we define the 2011 abrupt drop in water vapor and ozone as the mean difference between the annual average mixing ratios from 2012/13 and the annual average mixing ratios from 2010/11. This definition is chosen so that the maximum (minimum) in TTL concentrations reside in the earlier (later) periods (see Fig. 1). Abrupt drop mean differences are calculated at every three-dimensional location within the useful ranges of *Aura* MLS. Because of the sensitivity of radiative forcing calculations to the tropopause (Forster et al. 1997), we define a ''cutoff altitude'' at and above which we consider changes during the abrupt drop, and changes below the cutoff altitude are set to zero. The cutoff altitude is the three-dimensionally varying, monthly averaged cold-point tropopause. As sensitivity tests, we also vary the cutoff altitude by selecting it to be one or multiple levels above or below the CPT (MLS vertical levels are separated by ~1.3 log-pressure km). Varying the cutoff altitude demonstrates the sensitivity of changes relative to the tropopause level, which is particularly relevant because large perturbations associated with the 2011 abrupt drop are observed below the CPT but within the substratosphere.

The 2011 abrupt drop zonal-mean structures of percentage changes in water vapor and ozone are shown in Fig. 3. These results are shown on the Parallel Offline Radiative Transfer (PORT) model grid (described in appendix B) for direct comparison with model output results described in section 3b. For reference, the model's zonal and annual mean climatological tropopause is plotted (black dashed curve) along with the zonal mean 380-K isentropic surface (white dashed curve) calculated with MLS temperature data.

The largest percentage water vapor reductions during the 2011 abrupt drop (Fig. 3a) are observed in the TTL region, maximizing at the level nearest the CPT (82 hPa). Much of the recent emphasis on connections between changes in stratospheric water vapor and their links to climate has focused on these tropical regions (e.g., Randel et al. 2006; Rosenlof and Reid 2008; Solomon et al. 2010). A key result of this paper, however, is the substantial role of extratropical changes in water vapor that are associated with the tropical anomalies. Figure 3a shows that there is a ''wing'' behavior in the reductions of water vapor, with considerable reductions at higher latitudes in both hemispheres. These extratropical reductions, maximizing at 50°S and 40°N respectively, have important radiative influences (see sections 3b and 3c). These reductions appear to be associated with poleward quasi-isentropic transport away from anomalous upwelling in the tropics (Holton et al. 1995; Rosenlof et al. 1997; Randel and Jensen 2013). The 380-K isentropic surface (dashed white curve in Fig. 3a) is indicative of this, with water vapor reductions approximately following the adiabat and then sinking below it as the pole is approached in both hemispheres.

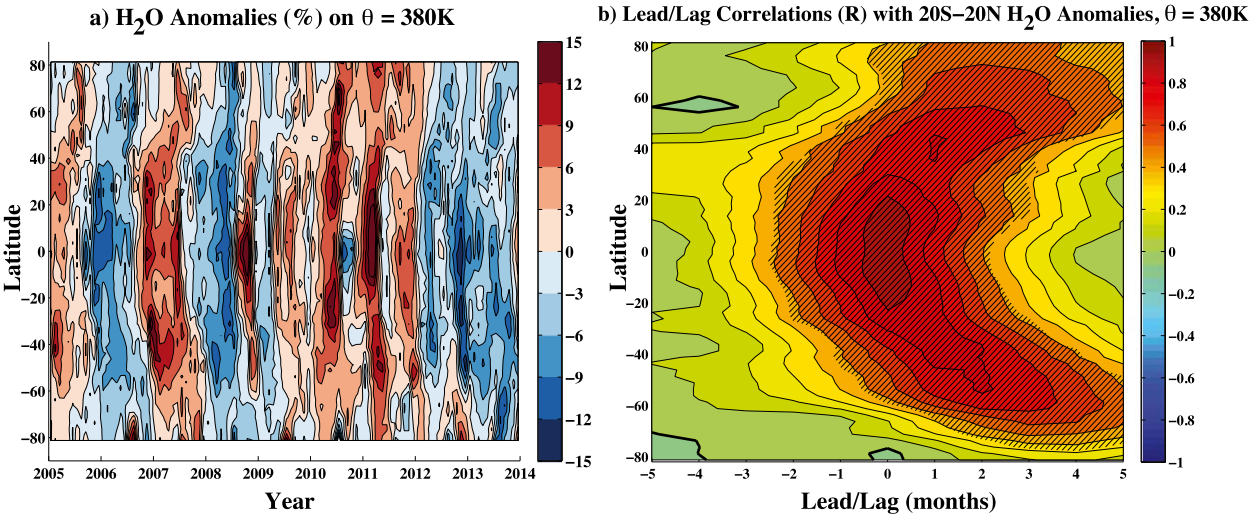

FIG. 4. (a) Zonal and monthly mean time–latitude cross section of deseasonalized water vapor anomalies (%) on the 380-K isentropic surface (denoted by dashed white line in Fig. 3). Contour intervals are 3%. (b) The monthly lead–lag correlation coefficients, on the 380-K isentropic surface, between the deseasonalized zonal and monthly mean time series of water vapor anomalies averaged over 20°S–20°N, and the zonal and monthly mean time series at each latitude. Contour intervals are every 0.1. The thick black contour denotes where $R = 0.0$. Hatching indicates significant correlations at 95% confidence, determined with a two-sided Student's t test and with the effective degrees of freedom adjusted to account for autocorrelation (see text). Data for (a) and (b) are drawn from the combined SWOOSH dataset from 2005 to 2013.

Water vapor anomalies on a time–latitude section of the 380-K surface [similar to Randel and Jensen (2013)] are plotted in Fig. 4a using SWOOSH data. Zonal-mean water vapor anomalies of up to ±15% originate at tropical latitudes during both the early and the late periods of the 2011 abrupt drop (2010/11 and 2012/13, respectively) and propagate poleward in time along the surface to the extratropics (see Fig. 3a). To analyze this propagation in greater detail, we compute the lead–lag cross-correlations between the zonal and monthly mean time series of deseasonalized water vapor anomalies on the 380-K isentropic surface averaged over 20°S—20°N, and the corresponding time series at each latitude bin (separated by every 2.5°) from 90°S to 90°N. The lead–lag correlation coefficients between these time series are shown in Fig. 4b. The significance of these correlations is computed using the two-sided Student's t test described in section 2a. Figure 4b shows that tropical anomalies are significantly correlated with anomalies propagating out of the tropics and poleward in both hemispheres, typically reaching 60° latitude in 3–4 months. This is consistent with the time scale of poleward isentropic propagation in this region estimated by Rosenlof et al. (1997). Results are qualitatively similar if we consider anomalies only during the 2011 abrupt drop period (2010–13), with extratropical anomalies lagging tropical anomalies by 1–4 months with significant correlations. In addition to this quasi-isentropic transport, horizontal mixing between the midlatitudes and tropics in the lower stratosphere may have also impacted the water vapor changes associated with the 2011 abrupt drop (e.g., Mote et al. 1998; Ploeger et al. 2011).

The ozone reductions during the 2011 abrupt drop (Fig. 3b) appear prominently in a shallow region of the TTL, and maximize from 30°S to the equator at 100 hPa. North of the equator there are slight increases in lower stratospheric ozone, showing that ozone changes are much less spatially extensive than the water vapor changes during the 2011 abrupt drop. This suggests that processes besides vertical advection, such as horizontal mixing and photochemistry, are likely impacting ozone's spatial distribution (Konopka et al. 2009; Ploeger et al. 2011). In contrast to the tropical reductions, ozone increases during the 2011 abrupt drop over the pole in Northern Hemisphere (NH) and also increases in the "collar" region of the jet stream (e.g., Randel et al. 2002) and poleward in the Southern Hemisphere (SH). This result appears to be consistent with an increased stratospheric circulation averaged over the abrupt drop period.

To investigate this further, we determine the linear congruence of the anomaly time series of temperature and ozone concentrations, averaged zonally and over 68–100 hPa, as in Thompson and Solomon (2009). Details of this analysis are found in appendix A. The analysis is intended to isolate the correlated nature of the ozone and temperature relationship in these atmospheric layers across latitude bands, with positive

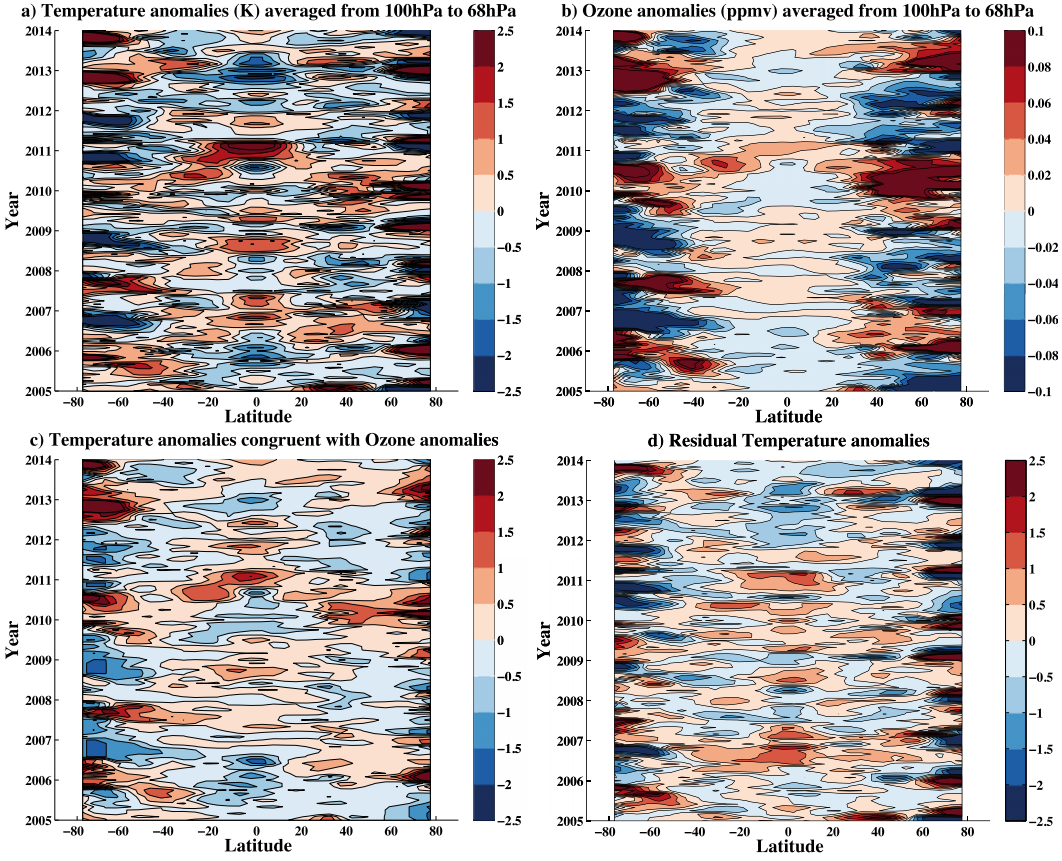

FIG. 5. Zonal and monthly mean time–latitude cross sections of (a) temperature anomalies (K) and (b) absolute ozone anomalies (ppmv), and (c) temperature anomalies congruent with ozone anomalies (K) [as computed from Eq. (A1)] and (d) the residual temperature anomalies (K) [i.e. the difference between (a) and (c)]. All quantities are averaged over 100–68 hPa from *Aura* MLS. Contour intervals are 0.5 K and 0.02 ppmv. Color bars saturate above ±2.5 K and ±0.1 ppmv for temperature and ozone, respectively.

temperature anomalies relating to positive ozone anomalies both dynamically and radiatively as discussed in section 2a (the analysis cannot distinguish between these physical processes). Results are shown in Fig. 5. The temperature anomalies congruent with ozone display a consistent pattern, with opposite signed anomalies between the equator and the poles, especially during periods of large temperature variability in the tropics (e.g., 2006, 2011, and 2013). These results support the hypothesis that increased stratospheric circulation played a role in tropical ozone reductions and polar ozone increases (Fig. 3b) during the 2011 abrupt drop period. This offsetting ozone variability between low and high latitudes has radiative consequences in the troposphere, which we discuss in sections 3b and 3c.

We note that the processes controlling water vapor and ozone variability are distinct, as discussed in section 2a. Water vapor anomalies originating in the TTL are largely set by the temperatures near the CPT and stratospheric water vapor is long lived, such that its abundance is conserved as parcels travel into the stratosphere away from locations of anomalous vertical motion (e.g., the tropical tape recorder signal). In contrast, the chemical lifetime for ozone decreases rapidly as air rises in the tropical lower stratosphere (Brasseur and Solomon 1986), such that ozone concentrations are not conserved as parcels travel away from the regions of upwelling or downwelling (e.g., Schoeberl et al. 2008). Observations from both species are consistent with an overall increase in stratospheric circulation between the two periods of the 2011 abrupt drop (2012/13 and 2010/11).

3. Radiation

a. *Methods*

The primary tool used herein to investigate the radiative influences of the 2011 abrupt drop in water vapor and ozone is the Parallel Offline Radiative Transfer

model (Conley et al. 2013), a configuration of the Community Atmosphere Model, version 4 (CAM4), in the Community Earth System Model (CESM1) which runs the radiative transfer code offline. The model uses seasonally evolving fixed-dynamical heating (FDH; Fels et al. 1980; Forster et al. 1997) to determine temperature adjustments (T_{adj}) and adjusted radiative forcing (RF) at the tropopause (IPCC 2013) associated with perturbations in chemical constituents (a description of the model and implementation details are found in appendix B). Use of PORT facilitates comparison to a wide range of studies using the CESM framework.

PORT results are compared to the line-by-line (LBL) model used in Solomon et al. (2010) in appendix C. Therein we also present an evaluation of PORT following the approach of Maycock and Shine (2012). Overall, there is good agreement between PORT and the LBL code, and PORT performs within the level of uncertainty found for other broadband models compared to the line-by-line model in Maycock and Shine (2012).

We perturb PORT using the definition of the 2011 abrupt drop described and analyzed in section 2b, imposing the three-dimensional absolute mixing ratio changes in water vapor and ozone above various cutoff altitudes. Our methodology is formulated to consistently apply observed constituent changes vertically in the model and account for the extreme radiative sensitivity to the tropopause altitude. Specifically, water vapor and ozone MLS gridded abrupt drop perturbations lie on a log pressure vertical grid relative to the log pressure height of the CPT, and are linearly interpolated to PORT's log pressure vertical grid relative to the log pressure height of PORT's tropopause. This method preserves the vertical distribution of changes in water vapor and ozone relative to the tropopause and thus the radiative effects of that distribution.

Water vapor and ozone perturbations are applied in separate runs to isolate their individual effects. We then linearly add water vapor and ozone outputs to obtain the total effect of their perturbations (there is a less than 1% quantitative difference between nonlinearly imposed and linearly added results). To determine both RF and radiative temperature changes associated with the 2011 abrupt drop in water vapor and ozone, PORT is run in two distinct modes, as follows:

1) RF is computed at the climatological tropopause assuming FDH in the stratosphere (all atmospheric layers above the CPT). In this mode the cutoff altitude is varied to determine the sensitivity of perturbations relative to the tropopause level. (RF results are shown in Figs. 7 and 8 and are discussed in sections 3c and 3d.)
2) In addition to the FDH stratospheric temperature adjustments in mode 1, temperatures below the CPT (within 400 hPa of the tropopause) are also allowed to adjust radiatively to the imposed composition perturbations, assuming FDH. In this mode water vapor and ozone perturbations are only imposed at and above the tropopause (the cutoff altitude is not varied). Radiative adjustments can be expected in the substratosphere just below the tropopause. While dynamical temperature adjustments would also be expected at altitudes below the tropopause in the real world, runs in this mode estimate the impact of radiation on temperatures alone. [Radiative temperature adjustment (hereafter simply "temperature adjustment") results are shown in Fig. 6 and are discussed in section 3b.]

b. *Radiative temperature adjustments*

Zonal-mean temperature adjustments associated with the 2011 abrupt drop perturbations in water vapor and ozone are shown in Fig. 6. The total zonal-mean temperature adjustment associated with the perturbations in both constituents is the sum of Figs. 6a and 6b (as noted in section 3a). As in Fig. 3, PORT's zonal and annual mean climatological tropopause is plotted for reference (black dashed curve).

Water vapor–related temperature adjustments (Fig. 6a) display a distinct pattern of radiative warming above the tropopause and radiative cooling below the tropopause. Because water vapor locally cools the TTL (Gettelman et al. 2004), reductions during the 2011 abrupt drop locally warm the layers above the tropopause. This local warming increases the layer emission temperatures and therefore implies a nonlocal warming response in the surrounding layers. However, in the case of water vapor the net nonlocal response below the tropopause (i.e., below levels where the perturbations are applied) is a cooling rather than a warming. This result suggests that another radiative effect, in particular a reduced exchange term in the layers below the tropopause due to the reductions in water vapor above the tropopause, is larger and more important than the aforementioned changes in the emission temperatures.

The largest local warming above the climatological tropical tropopause, about 0.4–0.5 K, is found at 70 hPa over the equator and near 100 hPa at 20°S and 20°N. A minimum in warming is found in the equatorial 100-hPa layer that arises from portions of the tropopause (here, the fixed cutoff altitude) lying above these levels over the Pacific warm pool region. Cooling occurs across the

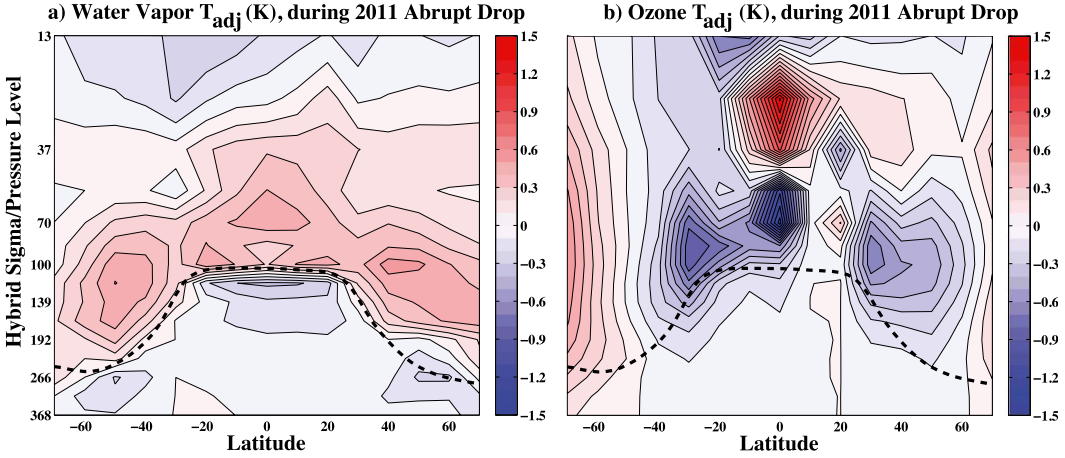

FIG. 6. Temperature adjustments (K) from radiative calculations using PORT and assuming fixed-dynamical heating. Results are associated with applications of three-dimensional perturbations (mean absolute differences between 2012/13 and 2010/11 concentrations) above the climatological tropopause to (a) water vapor and (b) ozone fields. The dashed black curve is the zonal and annual mean tropopause. Contour intervals are 0.1 K.

substratospheric levels just below the tropopause, with adjustments ranging from about −0.2 to −0.3 K from 20°S to 20°N at 118 hPa. Below this level, the cooling remains broad across tropical latitudes and is between −0.02 and −0.17 K over 192–139 hPa.

Temperature adjustments in the extratropical wings show a similar behavior to those in the tropics, but with larger swaths of warming above the tropopause in agreement with large absolute reductions in water vapor. There is deep warming above the tropopause in the extratropics, with adjustments between +0.3 and +0.55 K in the NH wing and between +0.35 and +0.5 K in the SH wing. While substantially contrasting with the warming above, cooling below the extratropical tropopause (adjustments between about −0.1 to −0.2 K) is weaker than that found in the tropical substratosphere. Here we note that although the extratropical percentage water vapor changes are smaller than those in the TTL, their radiative effect is similar in magnitude. This is because 1) at higher pressures the absolute concentration change in water vapor is large, 2) spectral absorption line widths are larger at higher pressures, and 3) the temperatures adjust through a larger depth above the tropopause in the extratropics than the tropics (as in Maycock et al. 2011). Thus extratropical water vapor reductions, which are linked in part to the quasi-isentropic poleward propagation of tropical anomalies, are important for the overall radiative signal associated with the 2011 abrupt drop.

Ozone-related temperature adjustments (Fig. 6b) show strong local radiative effects. Ozone reductions locally cool the atmosphere whereas ozone increases locally warm the atmosphere. Large cooling adjustments above the tropopause of between −0.3 and −1.45 K are found in the deep tropics, over 40°–20°S, and over 30°–50°N. These local radiative signals are largely dominated by shortwave absorption, with longwave emission changes playing a smaller role. Ozone reductions and the resulting local cooling reduce these layers' blackbody emission temperatures. This in turn reduces the longwave emission down into the troposphere, and results in cooling below the layers of ozone reductions (e.g., Grise et al. 2009). The majority of this nonlocal longwave exchange term cooling associated with the 2011 abrupt drop in ozone is found at the levels just below the tropical tropopause (Fig. 6b), leading to adjustment of about −0.2 K between the equator and 20°S at 118 hPa. Adjustments range from 0.0 to −0.2 K in other parts of the tropical substratosphere.

The lack of spatial coherence in the ozone signal (discussed in section 2b) impacts these nonlocal radiative effects, with warming adjustments over 10°–20°N, and cooling adjustments over 40°–30°S and 30°–50°N. Large high-latitude ozone increases—likely a consequence of increased stratospheric circulation during the 2011 abrupt drop (see Fig. 5 and discussion in section 2b)—are associated with local warming anomalies above the polar tropopause (NH ~+0.2 K and SH ~+0.5 K) that similarly reach into the layers below the tropopause.

The temperature adjustments associated with the 2011 abrupt drops in water vapor and ozone are of the same sign in the tropical substratosphere. The consequence of this is net radiative cooling just below the

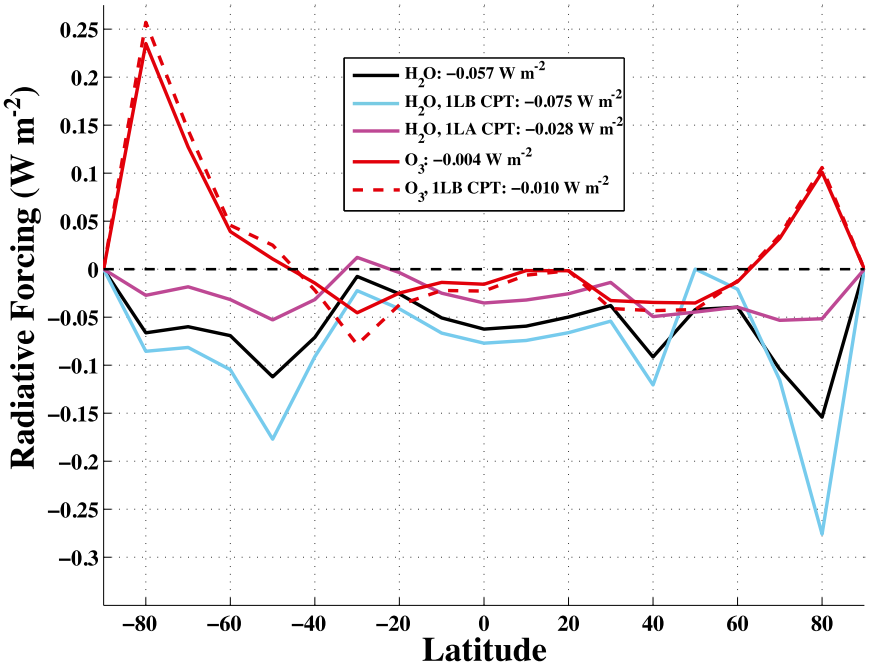

FIG. 7. Radiative forcing (W m^{-2}) by latitude from radiative calculations using PORT and assuming fixed-dynamical heating. Results are associated with applications of three-dimensional perturbations (mean absolute differences between 2012/13 and 2010/11 concentrations) to water vapor (black, blue, and magenta curves) and ozone (red curves) fields, respectively. Several lines are associated with perturbations applied one level above (1LA) or one level below (1LB) the model tropopause (CPT) to illustrate the radiative sensitivity to tropopause height (see text). The global average radiative forcing from each run is shown in the legend.

tropical tropopause varying from about −0.25 to −0.5 K. The mean total cooling associated with water vapor and ozone reductions at 118 hPa and averaged over 20°S–20°N is about 0.4 K. Lowering the cutoff level in these experiments produces a qualitatively similar result (not shown), with an increased magnitude of net radiative cooling adjustments that are located just below the tropical layers where the 2011 abrupt drop perturbations are applied.

c. *Radiative forcing associated with the 2011 abrupt drop*

Figure 7 shows the latitudinal structure of the calculated RFs associated with the 2011 abrupt drops in water vapor and ozone. The globally averaged RF from each run is reported in the legend. The global RF associated with the water vapor reductions with the tropopause as the cutoff altitude is −0.057 W m^{-2}, ~42% less than the forcing associated with the 2000 abrupt drop as reported in Solomon et al. (2010). The forcing difference is largely due to smaller water vapor changes in 2011 because of the shorter time scale of the 2011 abrupt drop compared with the 2000 abrupt drop (2-yr as opposed to 4-yr windows used to define the periods for mean differencing; see section 2b); water vapor reductions have not yet fully propagated into the middle-to-upper stratosphere (Fig. 3a) compared with the 2000 abrupt drop, leading to a shallower signal and smaller magnitude 2011 abrupt drop water vapor forcing. In the latter months in the 2011 abrupt drop period, water vapor concentrations began to climb, in contrast with the temporal structure of the 2000 abrupt drop. We consider the long-term changes in stratospheric water vapor (along with the role of the 2011 abrupt drop) and the associated radiative forcing in section 3d.

Negative RF is pronounced in the extratropical wing regions (Fig. 7); RF poleward of 35° accounts for ~57% of the cosine-weighted global radiative impact. Thus a large part of the radiative water vapor forcing associated with the 2011 abrupt drop is attributable to anomalies in the extratropics. Although not shown explicitly herein, examination of the latitudinal variation of the RF associated with 2000 abrupt drop [using the definition of Solomon et al. (2010)] reveals that extratropical water vapor reductions were similarly

TABLE 1. Global radiative forcing ($W m^{-2}$) associated with water vapor or ozone mean differences between specific periods (each row, described in text), determined with radiative calculations using PORT assuming fixed-dynamical heating. The cutoff altitude at and above which perturbations are applied is denoted by column (described in text), illustrating the radiative sensitivity of changes relative to the tropopause height.

Mean difference periods and constituent	Two levels below tropopause	One level below tropopause	Tropopause	One level above tropopause	Two levels above tropopause
H_2O (2012/13 minus 2010/11)	−0.094	−0.075	−0.057	−0.028	−0.010
O_3 (2012/13 minus 2010/11)	−0.014	−0.010	−0.004	−0.001	−0.001
H_2O (Aug 2004–Dec 2013 minus 1990–99, excluding Pinatubo)	—	−0.050	−0.045	−0.036	−0.029

important for the 2000 abrupt drop global radiative forcing, with changes over 65°–35°S and 35°–65°N accounting for ~42% of the cosine-weighted global radiative impact.

Figure 7 and Table 1 show the results from varying the cutoff altitude. By lowering the cutoff level and allowing deeper reductions in water vapor to perturb the climate system and affect radiative calculations, the global RF increases compared with calculations using the tropopause as the cutoff altitude (Table 1). The largest differences appear in the extratropical wings, where there are considerable observed reductions below the climatological tropopause. The tropical RF increases only slightly when deeper reductions are passed to the model, suggesting reduced tropopause sensitivity at lower latitudes, and emphasizing the importance of the depth that reductions reach at higher latitudes (e.g., Maycock et al. 2011). When raising the cutoff altitude, the RF signal is reduced across the globe (Table 1). With the exception of the contrasting small increases in water vapor just below the tropopause at 50°N, a notable portion of the observed water vapor reduction signal is found below the climatological tropopause in our abrupt drop definition (Fig. 3a) but is still in the substratospheric portion of the TTL. Because these substratospheric changes are likely to be radiatively important, applying constituent changes only above the tropopause (i.e., using the tropopause as the cutoff altitude, yielding RF = $-0.057\,W m^{-2}$) is conservative.

Ozone reductions in the TTL have two main radiative effects (Ramanathan and Dickinson 1979): 1) they locally reduce temperatures through the FDH temperature adjustment (Forster and Shine 1997), limiting LW fluxes downward through the tropopause, and 2) they nonlocally increase the SW fluxes penetrating into the troposphere. The LW flux reductions are the larger of these two competing effects associated with the 2011 abrupt drop perturbations, and the result is a net cooling of the tropical troposphere as shown in Fig. 7. The global RF associated with the 2011 abrupt drop in ozone is $-0.005\,W m^{-2}$, but a new finding in this study is that this near-zero result arises from offsetting negative RF at low latitudes and positive RF at high latitudes. Whereas the near-exact offset of ozone radiative forcing is not necessarily constrained to be so, the nature of stratospheric circulation with anomalous advective upwelling in the tropics correlated with anomalous advective downwelling at higher latitudes (e.g., Randel et al. 2002, their Fig. 5) suggests that ozone radiative effects during abrupt dynamically driven variability events should offset to some extent when averaging globally.

d. *Long-term changes in water vapor and 2011 abrupt drop implications*

In the preceding sections we have discussed the short-term radiative impacts of the large variability in water vapor during the 2011 abrupt drop. The extent to which RF associated with abrupt drops in water vapor cool surface climate and offset greenhouse gas warming is dependent not only on the spatial extent but also on the temporal extent of the reductions, compared to a reference value of water vapor. Short-term variability, such as the 4-yr period considered in this study's definition of the 2011 abrupt drop, will transiently force the climate system, whereas low water vapor concentrations in the longer term would result in prolonged forcing of the climate system (e.g., over time scales of a decade or more).

To examine the long-term changes in water vapor and their radiative effects in greater detail, we use observations from the SWOOSH dataset. Following Randel et al. (2009), the 2-yr period following the Pinatubo eruption (June 1991–May 1993) is excluded from each of the following analyses. We compute the mean differences between water vapor concentrations in the *Aura* MLS period (August 2004–December 2013) and in the decade prior to the 2000 abrupt drop (1990–99). Results are very similar if 1996–99 [the period employed in Solomon et al. (2010)] is instead used as the period prior to the 2000 abrupt drop, or if 2000–13 is used instead of the *Aura* MLS period alone following the 2000 abrupt drop. We consider only

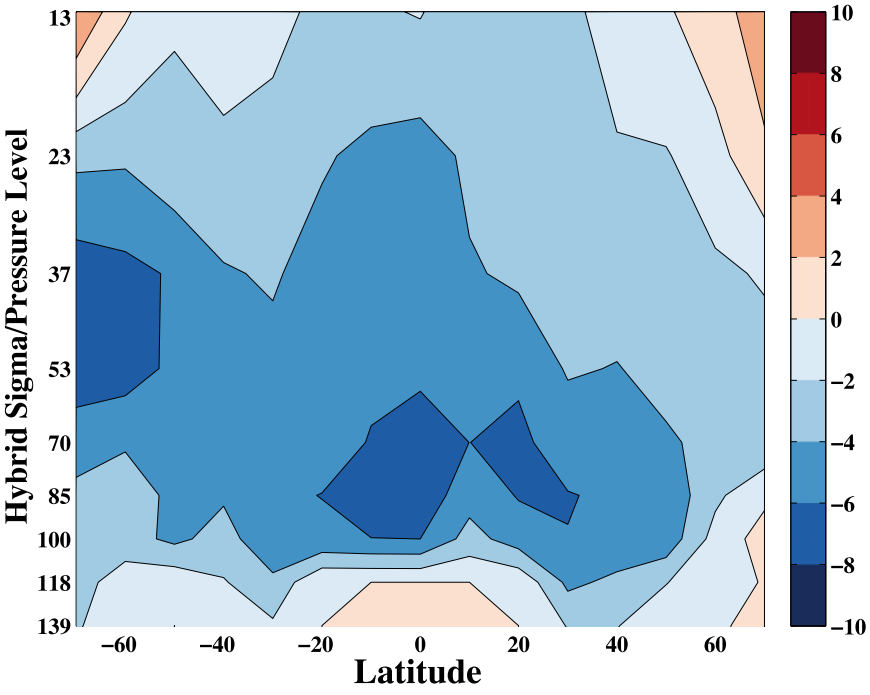

FIG. 8. Zonal-mean distribution of percentage mean water vapor differences between the *Aura* MLS period (Aug 2004–Dec 2013) and 1990–99 (excluding the 2-yr period following the Pinatubo eruption, Jun 1991–May 1993) using SWOOSH combined data. These changes are used to perturb the radiative transfer model (PORT) and thus are shown on the PORT grid for comparison with radiation results. Contour intervals are 2%.

mean differences observed at 100 hPa or above because HALOE observations (on which a portion of the pre-2005 SWOOSH water vapor data are based) below 100 hPa are of limited quality (Harries et al. 1996).

The absolute observed mean differences are used to perturb PORT following the methodology described in section 3a. The zonal-mean structure of these mean differences is shown in Fig. 8 on the PORT grid. Mean differences falling below 100 hPa in Fig. 8 indicate that at some longitude in that latitudinal band the PORT mean tropopause has a lower altitude than the *Aura* MLS mean tropopause. The adjusted RFs from the associated radiative calculations with PORT (assuming FDH in the stratosphere, mode 1 in section 3a) are shown in Table 1.

Figure 8 shows that through most of the stratosphere, water vapor concentrations are ~4%–8% lower in the *Aura* MLS period than in 1990–99. Adopting a cutoff altitude at the tropopause, the global RF associated with these changes is $-0.045\,\mathrm{W\,m^{-2}}$, as shown in Table 1. This forcing is smaller than the forcing associated with the 2000 abrupt drop as reported in Solomon et al. (2010), in part because the water vapor averaged over the *Aura* MLS period from 2004 to 2013 is higher than the period from June 2001 to May 2005 used in Solomon et al. (2010). For comparison, the average carbon dioxide radiative forcing between 2004–14 and 1990–99 as calculated by the NOAA Annual Greenhouse Gas Index (AGGI; Hofmann et al. 2006; Butler and Montzka 2015) is $+0.37\,\mathrm{W\,m^{-2}}$.

To illustrate the 2011 abrupt drop in the context of the long-term concentrations of water vapor, a time series of SWOOSH water vapor anomalies at 82 hPa and averaged over 30°S–30°N is shown in Fig. 9 (solid black curve). Anomalies are deseasonalized and are relative to the SWOOSH water vapor time mean over 1990–2013 (horizontal solid black line). The anomalies during the *Aura* MLS period are highlighted (solid blue curve) in Fig. 9, along with the 5-yr running mean at 82 hPa over 30°S–30°N for reference (solid gray curve). The time means of anomalies over 1990–99 and the *Aura* MLS period are shown as black dashed and blue dashed horizontal lines, respectively, whereas the time means of anomalies during the 2010/11 and 2012/13 periods of the 2011 abrupt drop are shown as red dashed horizontal lines. The global radiative forcing values (with the tropopause as the cutoff altitude) associated with the long-term changes in water vapor (RF1) and the 2011 abrupt drop (RF2) are shown on the right-hand side of the figure.

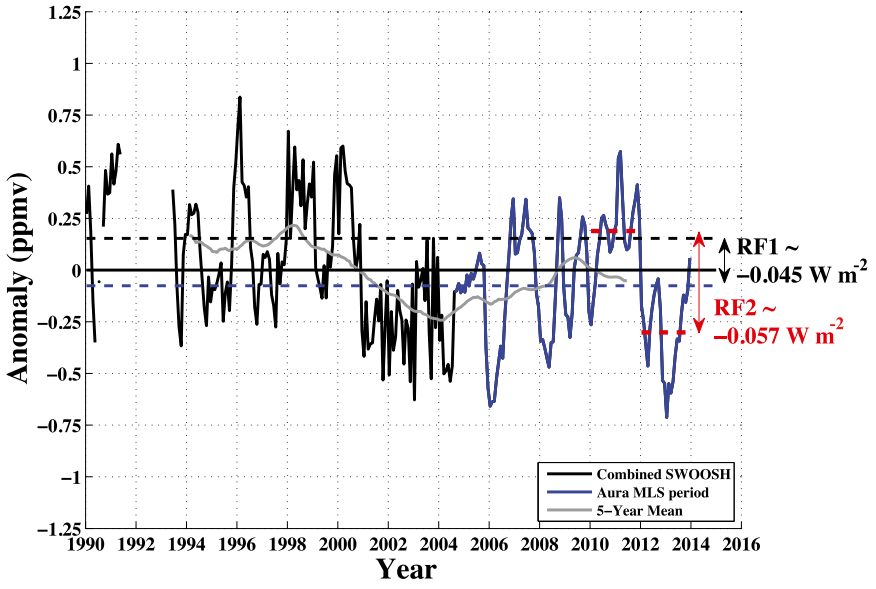

FIG. 9. Monthly time series of deseasonalized water vapor anomalies from the combined SWOOSH dataset averaged over 30°S–30°N at 82 hPa. The combined SWOOSH data product is a weighted mean of HALOE, *UARS* MLS, SAGE, and *Aura* MLS satellite measurements. The 2-yr period following the Pinatubo eruption (June 1991–May 1993) is excluded from these analyses. The 5-yr running mean anomaly is calculated from the SWOOSH combined product over 30°S–30°N at 82 hPa (gray curve). SWOOSH combined data during the *Aura* MLS period (Aug 2004–Dec 2013) are shown in the blue curve, while SWOOSH combined data prior to the *Aura* MLS period (Jan 1990–Jul 2004) are shown in the black curve. The solid black horizontal line denotes the mean of the SWOOSH combined data from 1990 to 2013, averaged over 30°S–30°N at 82 hPa. The dashed black curve indicates the average level of water vapor from 1990–99 relative to the SWOOSH combined data mean. The dashed blue horizontal line indicates the average level of water vapor during the *Aura* MLS period relative to the SWOOSH combined data mean. The dashed red horizontal lines indicate the average water vapor levels during 2010/11 and 2012/13, respectively, relative to SWOOSH combined data mean. The globally averaged radiative forcings associated with the total water vapor differences above the tropopause are shown on the right-hand side of the figure: RF1 between the *Aura* MLS period (blue dashed line) and 1990–99 (black dashed line), and RF2 between the 2010/11 and 2012/13 periods of the 2011 abrupt drop (red dashed lines).

Figure 9 shows the evolution of TTL water vapor concentrations since 1990. Following the 2000 abrupt drop, water vapor concentrations slowly rose toward their 1990–99 mean values, reaching a local maximum in September 2011. However, water vapor concentrations did not remain high; instead the occurrence of the 2011 abrupt drop over the next ~21 months reduced the mean water vapor propagating through the TTL, keeping stratospheric water vapor concentrations low relative to the 1990–99 levels (note that the 5-yr mean values remain close to the *Aura* MLS period mean following the 2011 abrupt drop). In the context of long-term changes in stratospheric water vapor, the role of the 2011 abrupt drop was to extend the period of relatively low concentrations after the 2000 abrupt drop and to prolong their radiative impacts. Whether water vapor concentrations following the 2011 abrupt drop will remain low has yet be determined; observations following 2013 will be needed to make this assessment.

4. Summary

Aura Microwave Limb Sounder (MLS) observations show that beginning in 2011 an abrupt drop in temperatures, water vapor, and ozone occurred in the tropical tropopause layer (TTL). Temperature, water vapor, and ozone are all significantly positively correlated over the 100–82-hPa levels and during the two years (2011 and 2012) of the abrupt drop event. The abrupt drop is likely related to increased stratospheric circulation and anomalous upwelling in the TTL (e.g., Dessler et al. 2013) enhanced by local ozone radiative feedback (e.g., Polvani and Solomon 2012) and is accompanied by positive ozone anomalies at higher latitudes that likely result from increased downwelling. In this study we have

focused on the radiative effects of water vapor and ozone changes associated with the 2011 abrupt drop. The global radiative forcing associated with the 2011 abrupt drops in water vapor and ozone as calculated by the Parallel Offline Radiative Transfer (PORT) model (Conley et al. 2013) are -0.057 and $-0.005\,\mathrm{W\,m^{-2}}$, respectively (Fig. 7), and similar values are obtained with an independent line-by-line code (-0.049 and $+0.003\,\mathrm{W\,m^{-2}}$; see Fig. C1). The radiative forcing varies by latitude in agreement with the latitudinal dependence of the ozone and water vapor abrupt drop patterns.

In this study we have shown several new results that have increased understanding of TTL abrupt drops and their radiative effects:

1) The quasi-isentropic poleward propagation of water vapor reductions during the 2011 abrupt drop led to considerable reductions in the extratropics, displaying a ''wing'' reduction behavior (Fig. 3). Reductions in extratropical water vapor concentrations contribute considerably to the global radiative impacts associated with the 2011 abrupt drop period, with ~57% of the global cosine-weighted radiative forcing attributable to reductions poleward of 35°.
2) Ozone reductions in the TTL during the 2011 abrupt drop are offset by high-latitude increases in ozone, congruent with temperature anomalies and consistent with increases in stratospheric circulation and anomalous ozone advection during the period. The radiative result of these anticorrelations during the 2011 abrupt drop is a near-zero global cosine-weighted radiative forcing, due to offsetting radiative impacts between the low and high latitudes. This offset appreciably reduces the overall global radiative impact of the ozone abrupt drop. Such behavior should be expected whenever large ozone variability is congruent with large temperature variability, related to increased or decreased stratospheric circulation (see Fig. 5 for useful diagnostics of such signatures).
3) The 2011 abrupt drops in TTL water vapor and ozone lead to same-signed cooling radiative temperature adjustments in the atmospheric layers just below the tropopause (Fig. 6). Purely radiative adjustments are between about -0.25 and $-0.5\,\mathrm{K}$ across the 192–118-hPa levels, in the radiatively dominated region referred to as the substratosphere (e.g., Thuburn and Craig 2002).

The magnitude of the radiative forcing associated with water vapor reductions is sensitive to the level chosen as the cutoff altitude (the level at and above which perturbations are considered), indicating that radiative calculations are very sensitive to constituent changes close to the tropopause (Forster et al. 1997). Selecting the tropopause as the cutoff altitude is conservative in calculating radiative forcing, as a large portion of observed water vapor reduction during the 2011 abrupt drop is found just below the cold-point tropopause (Fig. 3 and Table 1).

A consequence of the 2011 abrupt drop is prolonged low concentrations of stratospheric water vapor relative to the mean concentrations from 1990 to 1999. Although stratospheric water vapor appeared to be rising to near the mean levels prior to the 2000 abrupt drop, the 2011 abrupt drop prevented concentrations from reaching those levels for several more years (Fig. 9). Stratospheric water vapor concentrations from 1990 to 1999 were 4%–8% higher than concentrations during the *Aura* MLS period (August 2004–December 2013) as shown in Fig. 8, resulting in a global radiative forcing of $-0.045\,\mathrm{W\,m^{-2}}$ between these two periods (Table 1). Such forcing is about 12% of, and opposite in sign to, the carbon dioxide forcing over the period. This result suggests a significant climate role for stratospheric water vapor changes on decadal time scales between 1990 and 2014. Future forcing associated with stratospheric water vapor, and the long-term impacts of the 2011 abrupt drop, will depend on the future evolution of water vapor concentrations.

The use of fixed-dynamical heating to assess temperature changes permits understanding of pure radiative impacts, but this study has only assessed the first-order radiative feedback associated with dynamical driving of water vapor and ozone during the 2011 abrupt drop period. Dynamical changes themselves during the abrupt drop period (which are large) have not been accounted for in this study, and a dynamical feedback following the assessed radiative impacts has not been determined. In addition, this study has not accounted for other radiative active components of the climate system that may have been perturbed during the abrupt drop period, such as aerosols and clouds. More work is needed to understand the role of these constituents in affecting the TTL and surface climate during abrupt drops.

Acknowledgments. The lead author thanks Andrew Conley and Diane Ivy for assistance in implementing PORT. The lead author is grateful to Jeffrey Scott and Greg Shomo for maintaining the computing resources that were used to perform data analyses and models integrations. We thank two anonymous reviewers for their comments, which improved this manuscript. This work was supported by NASA Headquarters under the NASA Earth and Space Science Fellowship Program by

Grant NNX14AK83H. It was also supported by NSF Grants AGS-1342810 and -1461517.

APPENDIX A

Linear Decomposition of Ozone and Temperature Time Series

Following on Thompson and Solomon (2009), we decompose anomalous time series of temperature and ozone in the lower stratosphere. Specifically, the portion of zonal-mean temperature anomalies linearly congruent with ozone anomalies (T_{O_3}) is found with

$$T_{O_3}(y,t) = \frac{\overline{T(y,t)O_3(y,t)}}{\overline{[O_3(y,t)]^2}} O_3(y,t), \qquad \text{(A1)}$$

where O_3 are zonal-mean anomalies of ozone averaged over 68–100 hPa, T are zonal-mean anomalies of temperature averaged over 68–100 hPa, y is latitude dependence, t is time dependence, and the overbar denotes the time average. The fraction term in Eq. (A1) is the temporal regression of temperature anomalies onto ozone anomalies: a constant value at each latitude. Temperature anomalies can thus be divided into a linearly congruent portion (T_{O_3}) and a residual (such that $T = T_{O_3} + T_{residual}$). Residuals represent the portion of the temperature anomaly time series not correlated with ozone anomalies at particular latitudes. We perform this analysis with the *Aura* MLS data (from 2005 to 2013) described in section 2a. Anomalies, congruent temperatures, and residuals are plotted in Fig. 5.

APPENDIX B

PORT Description and Implementation

The Parallel Offline Radiative Transfer (PORT) model, described in Conley et al. (2013), employs radiative parameterizations developed by Briegleb (1992), Collins (1998), Ramanathan and Downey (1986), and Collins et al. (2002). There is no scattering in the longwave, and absorption and emission are calculated with a broadband model using eight longwave bands. In the shortwave, PORT uses parallel-plane compositions and a two-stream method to compute multiple scattering and absorption over 18 shortwave bands. More detailed descriptions of the model radiative calculations are found in Neale et al. (2010).

For each calculation, PORT is run for 16 months total: a 4-month spinup period and 12-month period for analysis. The 12-month analysis period is averaged to yield radiative forcing at the tropopause and temperature adjustments. Analysis time steps of just over 1.5 days are used to optimize model efficiency and accuracy (Conley et al. 2013), subsampled from 73 individual 30-min PORT calculation time steps. As noted in the PORT documentation (Conley et al. 2013), this choice of subsampling evenly samples all seasons and samples numerous solar angles representative of its annual variability. There is a less than 0.1% relative error between fully sampled model time step (72 daily) net fluxes and subsampled net fluxes averaged over the 12-month analysis period (see Table 1 in Conley et al. 2013). In total there are 240 analysis time steps in the 12-month analysis period.

PORT has 26 vertical levels from 992.6 to 3.54 in hybrid sigma/pressure coordinates. There are 16 total levels from 313.5 to 3.54 hPa. The model is run at a horizontal resolution of 10° latitude by 15° longitude. Constituent perturbations on the MLS horizontal grid (5° × 5°; see section 2a) are regridded to the PORT horizontal grid before they are applied to the model.

Background (boundary) model conditions, including temperature, water vapor, ozone, and clouds, are generated with a 16-month simulation of CESM1 [in accordance with the methodology outlined in Conley et al. (2013)] using a present-day climatology component-set (with monthly-fixed aerosols, fixed topography, and fixed present-day concentrations of methane, carbon dioxide, nitrous oxide, and chlorofluorocarbons). PORT runs are all-sky and include background cloud fields determined during the CESM1 simulations (the cloud fields are unchanged between PORT runs). Results are not sensitive to the background cloud fractions or optical depths.

PORT uses a seasonally evolving fixed-dynamical heating (FDH) approximation to calculate temperature adjustments to heating rate perturbations implied by perturbations in composition (Conley et al. 2013; Forster et al. 1997). Temperature adjustments (T_{adj}) assuming FDH are computed above a level specified by the user (taken in this study to be the model's climatological tropopause in run mode 1, or 400 hPa below the climatological tropopause in run mode 2; see section 3a), and reach quasi-equilibrium (with changes due to changes in climatological background compositions or seasonal solar heating) after the model's 4-month spinup period. The use of FDH also allows computation of adjusted radiative forcing (RF) as defined by the IPCC (2013). RF values are calculated from PORT by differencing the perturbed and unperturbed net radiative fluxes at the tropopause after

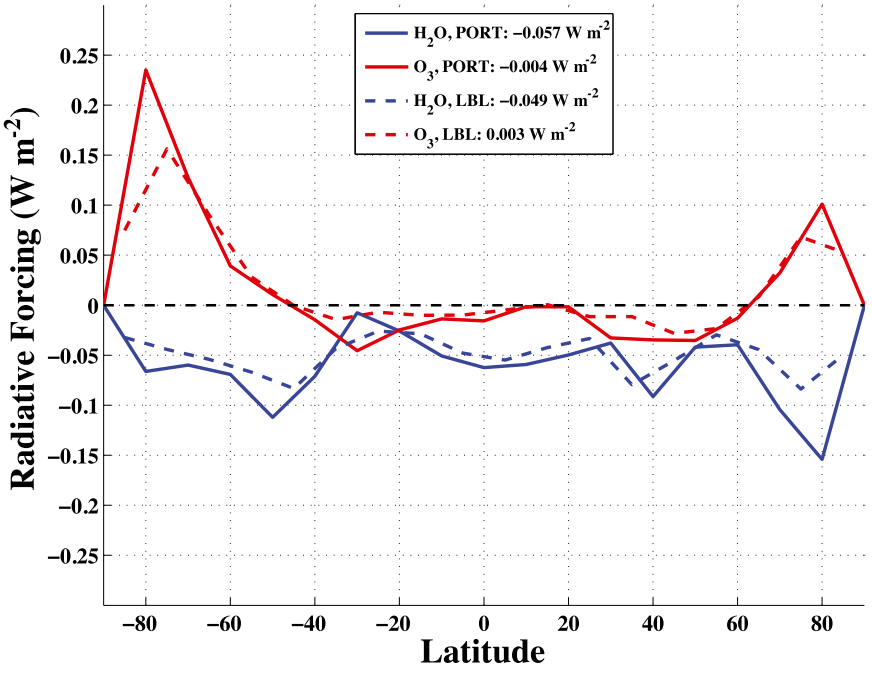

FIG. C1. Radiative forcing by latitude comparing results from the PORT (solid curves) and LBL (dashed curves) radiative codes. Results are associated with applications of three-dimensional perturbations (mean absolute differences between 2012/13 and 2010/11 concentrations) to water vapor (blue curves) and ozone (red curves) fields, respectively. All perturbations were applied at and above the CPT native to the models. The global average radiative forcing from each run is shown in the legend.

FDH adjustments, where the unperturbed fluxes are calculated from a control run with model background compositions. The model tropopause altitude varies by latitude, longitude, and month.

APPENDIX C

PORT Evaluation and Performance

PORT is compared to the line-by-line (LBL) code in Solomon et al. (2010). It is found that the magnitude of the adjusted RF kernel function is larger for PORT than the LBL, particularly at the tropopause levels, suggesting that in general PORT is more sensitive to changes in water vapor at and above the tropopause. For further validation, we compare the adjusted RF results reported herein (see section 3c) computed with PORT to those computed with the LBL model (Fig. C1). Consistent with the kernel function comparison, globally averaged RF associated with the abrupt drop in water vapor is smaller in magnitude for LBL results than for PORT results, but the latitudinal patterns in both model results are consistent. Similarly, for ozone, RF is smaller in magnitude in the LBL results but similar in spatial pattern. Weaker magnitudes could arise due to differences in model background concentrations, radiation parameterizations, or gridding differences.

Previously, Maycock and Shine (2012) examined the instantaneous radiative forcing calculation uncertainties associated with stratospheric water vapor changes by comparing a LBL radiative model and three broadband radiative models. Setting the background levels of stratospheric (from the CPT to 3.54 hPa) water vapor uniformly to 3 ppmv, they perturbed their atmosphere by adding 0.7 ppmv uniformly in the stratosphere and calculated the resulting instantaneous radiative forcing (RF_{inst}) at the tropopause. For their LBL model (averaged for a standard tropical profile) they found RF_{inst} = 0.260 W m^{-2}, while the broadband codes RF_{inst} differed nonsystematically by up to ±40%. Major differences/uncertainties likely arise from water vapor transmittance parameterizations. For comparison, we repeat the Maycock and Shine (2012) methodology by setting the stratospheric water vapor background in PORT to 3 ppmv and then perturb it by uniformly adding 0.7 ppmv. Averaging over the tropics (20°S–20°N), we find that PORT RF_{inst} = 0.189 W m^{-2}, which is ~27% smaller RF_{inst} than the Maycock and Shine (2012) reported LBL model forcing from the same water vapor

perturbation. This forcing is within the range of broadband code uncertainties described in Maycock and Shine (2012) and is similar (within 0.02 $W m^{-2}$) to the results of the radiative transfer code of Zhong and Haigh (1995) based on a common radiation scheme (Morcrette 1991). This gives confidence that PORT is performing similarly to typical broadband codes, and simultaneously cautions that there are some uncertainties with PORT radiative forcing calculations compared with LBL calculations.

REFERENCES

Bandoro, J., S. Solomon, A. Donohoe, D. W. J. Thompson, and B. D. Santer, 2014: Influences of the Antarctic ozone hole on Southern Hemisphere summer climate change. *J. Climate*, **27**, 6245–6264, doi:10.1175/JCLI-D-13-00698.1.

Brasseur, G., and S. Solomon, 1986: *Aeronomy of the Middle Atmosphere.* Springer, 452 pp.

Bretherton, C., M. Widmann, V. Dymnikov, J. Wallace, and I. Bladé, 1999: The effective number of spatial degrees of freedom of a time-varying field. *J. Climate*, **12**, 1990–2009, doi:10.1175/1520-0442(1999)012<1990:TENOSD>2.0.CO;2.

Briegleb, B. P., 1992: Delta-Eddington approximation for solar radiation in the NCAR Community Climate Model. *J. Geophys. Res.*, **97**, 7603–7612, doi:10.1029/92JD00291.

Butler, J. H., and S. A. Montzka, 2015: The NOAA Annual Greenhouse Gas Index (AGGI). [Available online at http://www.esrl.noaa.gov/gmd/aggi/aggi.html.]

Chae, J. H., and S. C. Sherwood, 2007: Annual temperature cycle of the tropical tropopause: A simple model study. *J. Geophys. Res.*, **112**, D19111, doi:10.1029/2006JD007956.

Collins, W. D., 1998: A global signature of enhanced shortwave absorption by clouds. *J. Geophys. Res.*, **103**, 31 669–31 679, doi:10.1029/1998JD200022.

——, J. K. Hackney, and D. P. Edwards, 2002: An updated parameterization for infrared emission and absorption by water vapor in the National Center for Atmospheric Research Community Atmosphere Model. *J. Geophys. Res.*, **107**, 4664, doi:10.1029/2001JD001365.

Conley, A. J., J.-F. Lamarque, F. Vitt, W. D. Collin, and J. Kiehl, 2013: PORT, a CESM tool for the diagnosis of radiative forcing. *Geosci. Model Dev.*, **6**, 469–476, doi:10.5194/gmd-6-469-2013.

Davis, S. M., and K. H. Rosenlof, 2013: SWOOSH: Stratospheric water and ozone satellite homogenized data set. [Available online at http://www.esrl.noaa.gov/csd/groups/csd8/swoosh/.]

Dessler, A. E., M. R. Schoeberl, T. Wang, S. M. Davis, and K. H. Rosenlof, 2013: Stratospheric water vapor feedback. *Proc. Natl. Acad. Sci. USA*, **110**, 18 087–18 091, doi:10.1073/pnas.1310344110.

——, ——, ——, ——, ——, and J.-P. Vernier, 2014: Variations of stratospheric water vapor over the past three decades. *J. Geophys. Res. Atmos.*, **119**, 12 588–12 598, doi:10.1002/2014JD021712.

Dhomse, S., M. Weber, and J. Burrows, 2008: The relationship between tropospheric wave forcing and tropical lower stratospheric water vapor. *Atmos. Chem. Phys.*, **8**, 471–480, doi:10.5194/acp-8-471-2008.

Fels, S. B., J. D. Mahlman, M. D. Schwarzkopf, and R. W. Sinclair, 1980: Stratospheric sensitivity to perturbations in ozone and carbon dioxide: Radiative and dynamical response. *J. Atmos. Sci.*, **37**, 2265–2297, doi:10.1175/1520-0469(1980)037<2265:SSTPIO>2.0.CO;2.

Folkins, I., M. Loewenstein, J. Podolske, S. J. Oltmans, and M. Proffitt, 1999: A barrier to vertical mixing at 14 km in the tropics: Evidence from ozonesondes and aircraft measurements. *J. Geophys. Res.*, **104** (D18), 22 095–22 102, doi:10.1029/1999JD900404.

——, S. J. Oltmans, and A. M. Thompson, 2000: Tropical convective outflow and near surface equivalent potential temperatures. *Geophys. Res. Lett.*, **27**, 2549–2552, doi:10.1029/2000GL011524.

——, P. Bernath, C. Boone, G. Lesins, N. Livesey, A. M. Thompson, K. Walker, and J. C. Witte, 2006: Seasonal cycles of O_3, CO, and convective outflow at the tropical tropopause. *Geophys. Res. Lett.*, **33**, L16802, doi:10.1029/2006GL026602.

Forster, P. M., and K. P. Shine, 1997: Radiative forcing and temperature trends from stratospheric ozone changes. *J. Geophys. Res.*, **102**, 10 841–10 855, doi:10.1029/96JD03510.

——, and ——, 1999: Stratospheric water vapour changes as a possible contributor to observed stratospheric cooling. *Geophys. Res. Lett.*, **26**, 3309–3312, doi:10.1029/1999GL010487.

——, and ——, 2002: Assessing the climate impacts of trends in stratospheric water vapour. *Geophys. Res. Lett.*, **29**, 1086–1089, doi:10.1029/2001GL013909.

——, R. S. Freckleton, and K. P. Shine, 1997: On aspects of the concept of radiative forcing. *Climate Dyn.*, **13**, 547–560, doi:10.1007/s003820050182.

Fueglistaler, S., A. E. Dessler, T. J. Dunkerton, I. Folkins, Q. Fu, and P. W. Mote, 2009: Tropical tropopause layer. *Rev. Geophys.*, **47**, RG1004, doi:10.1029/2008RG000267.

——, P. H. Haynes, and P. M. Forster, 2011: The annual cycle in lower stratospheric temperatures revisited. *Atmos. Chem. Phys.*, **11**, 3701–3711, doi:10.5194/acp-11-3701-2011.

Gettelman, A., and Coauthors, 2004: Radiation balance of the tropical tropopause layer. *J. Geophys. Res.*, **109**, D07103, doi:10.1029/2003JD004190.

Grise, K. M., D. W. J. Thompson, and P. M. Forster, 2009: On the role of radiative processes in stratosphere–troposphere coupling. *J. Climate*, **22**, 4154–4161, doi:10.1175/2009JCLI2756.1.

Harries, J. E., and Coauthors, 1996: Validation of measurements of water vapor from the Halogen Occultation Experiment (HALOE). *J. Geophys. Res.*, **101** (D6), 10 205–10 216, doi:10.1029/95JD02933.

Hegglin, M. I., and Coauthors, 2013: SPARC data initiative: Comparison of water vapor climatologies from international satellite limb sounders. *J. Geophys. Res. Atmos.*, **118**, 11 824–11 846, doi:10.1002/jgrd.50752.

Hofmann, D. J., J. H. Butler, E. J. Dlugokencky, J. W. Elkins, K. Masarie, S. A. Montzka, and P. Tans, 2006: The role of carbon dioxide in climate forcing from 1979 to 2004: Introduction of the Annual Greenhouse Gas Index. *Tellus*, **58B**, 614–619, doi:10.1111/j.1600-0889.2006.00201.x.

Holton, J. R., P. H. Haynes, M. E. McIntyre, A. R. Douglass, R. B. Rood, and L. Pfister, 1995: Stratosphere–troposphere exchange. *Rev. Geophys.*, **33**, 403–439, doi:10.1029/95RG02097.

IPCC, 2013: *Climate Change 2013: The Physical Science Basis.* T. J. Stocker et al., Eds., Cambridge University Press, 1535 pp. [Available online at https://www.ipcc.ch/report/ar5/wg1/.]

Joshi, M. M., and G. S. Jones, 2009: The climatic effects of the direct injection of water vapour into the stratosphere by large volcanic eruptions. *Atmos. Chem. Phys.*, **9**, 6109–6118, doi:10.5194/acp-9-6109-2009.

——, M. J. Webb, A. C. Maycock, and M. Collins, 2010: Stratospheric water vapour and high climate sensitivity in a version of the HadSM3 climate model. *Atmos. Chem. Phys.*, **10**, 7161–7167, doi:10.5194/acp-10-7161-2010.

Konopka, P., J Grooß, F. Plöger, and R. Müller, 2009: Annual cycle of horizontal in-mixing into the lower tropical stratosphere. *J. Geophys. Res.*, **114**, D19111, doi:10.1029/2009JD011955.

Lamarque, J., and S. Solomon, 2010: Impact of changes in climate and halocarbons on recent lower stratosphere ozone and temperature trends. *J. Climate*, **23**, 2599–2611, doi:10.1175/2010JCLI3179.1.

Livesey, N. J., and Coauthors, 2011: Version 3.3 level 2 data quality and description document. Doc. JPL D-33509, Jet Propulsion Laboratory, Pasadena, CA, 156 pp. [Available online at http://mls.jpl.nasa.gov/data/v3-3_data_quality_document.pdf.]

Maycock, A. C., and K. P. Shine, 2012: Stratospheric water vapor and climate: Sensitivity to the representation in radiation codes. *J. Geophys. Res.*, **117**, D13102, doi:10.1029/2012JD017484.

——, ——, and M. M. Joshi, 2011: The temperature response to stratospheric water vapour changes. *Quart. J. Roy. Meteor. Soc.*, **137**, 1070–1082, doi:10.1002/qj.822.

——, M. M. Joshi, K. P. Shine, S. M. Davis, and K. H. Rosenlof, 2014: The potential impact of changes in lower stratospheric water vapour on stratospheric temperatures over the past 30 years. *Quart. J. Roy. Meteor. Soc.*, **140**, 2176–2185, doi:10.1002/qj.2287.

Morcrette, J. J., 1991: Radiation and cloud radiative properties in the ECMWF operational forecast model. *J. Geophys. Res.*, **96**, 9121–9132, doi:10.1029/89JD01597.

Mote, P. W., and Coauthors, 1996: An atmospheric tape recorder: The imprint of tropical tropopause temperatures on stratospheric water vapor. *J. Geophys. Res.*, **101**, 3989–4006, doi:10.1029/95JD03422.

——, T. J. Dunkerton, M. E. McIntyre, E. A. Ray, P. H. Haynes, and J. M. Russell III, 1998: Vertical velocity, vertical diffusion, and dilution by midlatitude air in the tropical lower stratosphere. *J. Geophys. Res.*, **103** (D8), 8651–8666, doi:10.1029/98JD00203.

NASA, 2006: Missions: Aura. *Earth Science Reference Handbook*, C. L. Parkinson, A. Ward, and M. D. King, Eds., NASA, 101–117.

Neale, R. B., and Coauthors, 2010: Description of the NCAR Community Atmosphere Model (CAM 4.0). NCAR Tech. Note NCAR/TN-485+STR, 212 pp. [Available online at www.cesm.ucar.edu/models/ccsm4.0/cam/docs/description/cam4_desc.pdf.]

Ploeger, F., and Coauthors, 2011: Insight from ozone and water vapour on transport in the tropical tropopause layer (TTL). *Atmos. Chem. Phys.*, **11**, 407–419, doi:10.5194/acp-11-407-2011.

Polvani, L. M., and S. Solomon, 2012: The signature of ozone depletion on tropical temperature trends, as revealed by their seasonal cycle in model integrations with single forcings. *J. Geophys. Res.*, **117**, D17102, doi:10.1029/2012JD017719.

Ramanathan, V., and R. E. Dickinson, 1979: The role of stratospheric ozone in the zonal and seasonal radiative energy balance of the Earth–troposphere system. *J. Atmos. Sci.*, **36**, 1084–1104, doi:10.1175/1520-0469(1979)036<1084:TROSOI>2.0.CO;2.

——, and P. Downey, 1986: A nonisothermal emissivity and absorptivity formulation for water vapor. *J. Geophys. Res.*, **91**, 8649–8666, doi:10.1029/JD091iD08p08649.

Randel, W. J., and E. J. Jensen, 2013: Physical processes in the tropical tropopause layer and their roles in a changing climate. *Nat. Geosci.*, **6**, 169–176, doi:10.1038/ngeo1733.

——, and F. Wu, 2015: Variability of zonal mean tropical temperatures derived from a decade of GPS radio occultation data. *J. Atmos. Sci.*, **72**, 1261–1275, doi:10.1175/JAS-D-14-0216.1.

——, ——, and R. Stolarski, 2002: Changes in column ozone correlated with stratospheric EP flux. *J. Meteor. Soc. Japan*, **80**, 849–862, doi:10.2151/jmsj.80.849.

——, ——, H. Vömel, G. E. Nedoluha, and P. Forster, 2006: Decreases in stratospheric water vapor after 2001: Links to changes in the tropical tropopause and the Brewer–Dobson circulation. *J. Geophys. Res.*, **111**, D12312, doi:10.1029/2005JD006744.

——, and Coauthors, 2009: An update of observed stratospheric temperature trends. *J. Geophys. Res.*, **114**, D02107, doi:10.1029/2008JD010421.

Rosenlof, K. H., and G. C. Reid, 2008: Trends in the temperature and water vapor content of the tropical lower stratosphere: Sea surface connection. *J. Geophys. Res.*, **113**, D06107, doi:10.1029/2007JD009109.

——, A. F. Tuck, K. K. Kelly, J. M. Russell III, and M. P. McCormick, 1997: Hemispheric asymmetries in water vapor and inferences about transport in the lower stratosphere. *J. Geophys. Res.*, **102** (D11), 13 213–13 234, doi:10.1029/97JD00873.

Santer, B. D., T. M. L. Wigley, J. Boyle, D. J. Gaffen, J. Hnilo, D. Nychka, D. Parker, and K. Taylor, 2000: Statistical significance of trends and trend differences in layer-average atmospheric temperature time series. *J. Geophys. Res.*, **105** (D6), 7337–7356, doi:10.1029/1999JD901105.

Schoeberl, M. R., and Coauthors, 2008: QBO and annual cycle variations in tropical lower stratosphere gases from HALOE and *Aura* MLS observations. *J. Geophys. Res.*, **113**, D05301, doi:10.1029/2007JD008678.

Shindell, D. T., 2001: Climate and ozone response to increased stratospheric water vapor. *Geophys. Res. Lett.*, **28**, 1551–1554, doi:10.1029/1999GL011197.

Solomon, S., K. H. Rosenlof, R. W. Portmann, J. S. Daniel, S. M. Davis, T. J. Sanford, and G.-K. Plattner, 2010: Contributions of stratospheric water vapor to decadal changes in the rate of global warming. *Science*, **327**, 1219–1223, doi:10.1126/science.1182488.

Stuber, N., M. Ponater, and R. Sausen, 2001: Is the climate sensitivity of ozone perturbations enhanced by stratospheric water vapor feedback? *Geophys. Res. Lett.*, **28**, 2887–2890, doi:10.1029/2001GL013000.

Tegtmeier, S., and Coauthors, 2013: SPARC data initiative: A comparison of ozone climatologies from international satellite limb sounders. *J. Geophys. Res. Atmos.*, **118**, 12 229–12 247, doi:10.1002/2013JD019877.

Thompson, D. W. J., and S. Solomon, 2009: Understanding recent stratospheric climate change. *J. Climate*, **22**, 1934–1943, doi:10.1175/2008JCLI2482.1.

Thuburn, J., and G. C. Craig, 2002: On the temperature structure of the tropical substratosphere. *J. Geophys. Res.*, **107** (D2), doi:10.1029/2001JD000448.

Tian, W., M. P. Chipperfield, and L. Daren, 2009: Impact of increasing stratospheric water vapor on ozone depletion and temperature change. *Adv. Atmos. Sci.*, **26**, 423–437, doi:10.1007/s00376-009-0423-3.

Urban, J., S. Lossow, G. Stiller, and W. Read, 2014: Another drop in water vapor. *Eos, Trans. Amer. Geophys. Union*, **95**, 245–246, doi:10.1002/2014EO270001.

Zhong, W. Y., and J. D. Haigh, 1995: Improved broad-band emissivity parameterization for water vapor cooling rate calculations. *J. Atmos. Sci.*, **52**, 124–138, doi:10.1175/1520-0469(1995)052<0124:IBEPFW>2.0.CO;2.